Applied Catalysis A, General 624 (2021) 118296

Contents lists available at ScienceDirect

Applied Catalysis A, General

journal homepage: www.elsevier.com/locate/apcata

Ethylene oligomerization on nickel catalysts on a solid acid support: From New mechanistic insights to tunable bifunctionality

Elsa Koninckx [a], Pedro S.F. Mendes [b], Joris W. Thybaut [b], Linda J. Broadbelt [a,*]

[a] Department of Chemical and Biological Engineering, Northwestern University, McCormick School of Engineering and Applied Science, 2145 Sheridan Road, Evanston, IL, 60208, United States
[b] Laboratory for Chemical Technology, Ghent University, Technologiepark 125, Ghent, 9052, Belgium

ARTICLE INFO

Keywords:
Ethylene oligomerization
Catalysis
Zeolite
Nickel
Bifunctional

ABSTRACT

Light alkene oligomerization on heterogeneous acidic catalysts is widely and successfully used in current commercial processes. However, ethylene oligomerization remains inefficient due to ethylene's inability to form reaction intermediates to a sufficient extent on acid sites. Adding Ni(II) on solid acids can more efficiently catalyze ethylene oligomerization and selectively produce butenes to fuel range products. The review proposes a complete and detailed mechanism of heterogenous Ni-catalyzed oligomerization, whose structures are supported by combining various studies throughout recent literature, and focuses on the bifunctional effects of the nickel and acid sites on ethylene oligomerization. Using experiments, first-principles calculations, and kinetic modeling, Ni^{2+} has been shown to selectively oligomerize ethylene to light, linear alkenes via the Cossee-Arlman mechanism, while Brønsted H^{+} sites catalyze further alkylation, cracking, and isomerization reactions. The effects of reaction conditions and catalyst properties on selectivity and activity for oligomerization are systematically discussed. Tuning the relative nickel-to-acid site ratio and the framework support can allow for an optimal catalyst design directed towards desirable products.

1. Introduction

Ethylene and other light alkenes (e.g. propene, butene) are the oligomerization building blocks for producing linear and branched higher olefins found in a wide range of products including plastics (C4-C6), petrochemicals (C4-C10), liquid fuels (C5-C20), and lubricants (C10-C20) (Fig. 1) [1–6]. The state-of-the-art processes for ethylene oligomerization rely on organic solvents and homogenous catalysts [6,7]. These include trialkyl-aluminum (Chevron, Ineos) and nickel complexes (Shell, UOP) [1,8–10], for which the reaction mechanism is well-known [7]. Due to its advantages over homogeneous catalysis, including the potential for inexpensive separation, solvent-free operations, and easy catalyst recycling, significant research efforts are presently focusing on using heterogenous catalysis for light olefin oligomerization. Additionally, ethylene oligomerization via homogenous catalysis is mainly utilized for linear olefins (LAO) production and there is little flexibility in altering the product distribution to respond to market demands for fuels and chemicals. However, a bifunctional heterogeneous catalyst can produce a wide variety of linear and branched product distributions depending on reaction conditions and catalyst properties.

Alkene oligomerization over heterogenous acid catalysts, especially zeolites, has been driven to produce distillate quality fuels for decades [2,3,11–13]. However, due to the very unstable primary carbenium ion obtained from ethylene protonation, its overall reactivity with acid sites is very low compared to other small alkenes [1,14,15]. Transition metal ions can act similarly to homogenous organometallic catalysts when deposited on a support and promote the reactivity of ethylene. Ethylene

Abbreviations: ASA, amorphous silica-alumina; DAE, desorption activation energy; DFT, density functional theory; DRIFTS, diffuse reflectance infrared Fourier transform spectroscopy; DRUV, diffuse reflectance UV–vis; EPR, electron paramagnetic resonance; EXAFS, extended X-ray absorption fine structure; FTIR, Fourier transform infrared; H+, acid site; IR, infrared; LAO, linear-alpha olefins; MOF, metal-organic framework; Ni, nickel; PCP, protonated cyclopropane; SEMK, Single-Event MicroKinetic; TOF, turnover frequency; wt.%, weight percent; XAFS, X-ray absorption fine structure; XANES, X-ray absorption near edge structure; XAS, X-ray absorption spectroscopy; XPS, X-ray photoelectron spectroscopy.

* Corresponding author.
E-mail addresses: ekoninckx@u.northwestern.edu (E. Koninckx), pedro.mendes@ugent.be (P.S.F. Mendes), joris.thybaut@ugent.be (J.W. Thybaut), broadbelt@northwestern.edu (L.J. Broadbelt).

https://doi.org/10.1016/j.apcata.2021.118296
Received 27 March 2021; Received in revised form 25 July 2021; Accepted 26 July 2021
Available online 28 July 2021

is initially converted into larger alkenes on the metal site, which can then more easily undergo further acid-catalyzed reactions via more stable secondary and tertiary carbenium ions. The concept of combining a metal and zeolite for oligomerization is not new; it has been explored since at least the 1970s [16–19]. Transition metals for ethylene oligomerization have been studied including nickel, cobalt, and iron homogenous 2-(2-pyridyl)quinoxaline catalysts as well as nickel, rhodium, and palladium heterogeneous zeolite catalysts [16,20]. Based on comparisons among metals, nickel distinguished itself as a highly active, selective, stable, abundant, and inexpensive transition metal, which can be seen in its applications in industry and its primary focus in oligomerization literature. Initial heterogenous nickel-acid studies were done on silica-alumina [17,21,22] and zeolite Y [23–26], and since then have quickly expanded to cover other zeolite structures and mesoporous supportsc [1,27]. Nickel supports, such as zeolite BEA, mesoporous MCM, and metal-organic frameworks (MOFs), are used in more recent studies to address the early issues of heterogenous nickel catalysts, such as pronounced deactivation and low activity. Operating conditions and summaries of catalytic performance for the studies are discussed throughout but are also brought together in Table 1 at the end of the review.

Looking at contributions with broad scope, recent reviews on Ni dimerization and oligomerization were published by Hulea [1] and Ghashghaee [28] in 2018 and Olivier-Bourbigou et al. in 2020 [7]. Hulea and Ghashghaee both covered a broad range of ethylene oligomerization catalysts. Hulea focused on butene, propylene, and aromatic products. Ghashghaee focused on various transition metal catalysts and metathesis chemistry. Olivier-Bourbigou et al.'s review covered a large scope on Ni-based oligomerization, including the early history, industrial development, homogenous catalysis studies, as well as heterogenous catalysis studies. Most of the review remained focused on the more familiar homogenous catalysis, which often exhibit similarities to their heterogenous counterparts, but still differ due to framework and environment differences. To summarize, these reviews highlight recent studies and acknowledge the effect of the active site ratios and support porosity effects. However, a full understanding of the heterogenous Ni-acid mechanistic details has remained elusive. Even in a comprehensive review of nickel-promoted solid alumina supports published by Finiels et al. in 2014 [1], no strong agreement could be reached in the community about the nickel state, active site activation, oligomerization mechanism, nor application of comprehensive kinetic modeling or density functional theory (DFT). Yet, in the past five years there have been great advances in our understanding of bifunctional nickel and acid catalysts. This is likely in part due to a modern world-wide interest in converting inexpensive and abundant hydrocarbons associated with natural gas into liquid fuels [29–31].

The aim of this review is to provide a critical overview of the current knowledge regarding ethylene oligomerization on Ni-acid heterogenous catalysts. Recently published literature studies using experimental analysis, such as *in situ* IR and X-ray spectroscopy, as well as energy calculations have made it possible to distinguish the Ni-site Cossee-Arlman mechanism (over the metallacycle) and link the Ni and acid contributions to product selectivity. A detailed oligomerization mechanism for nickel and acid active sites based on recent findings is presented and discussed (Section 2). The proposed mechanism is a result of coupling what many others have uncovered but have never been analyzed together. The effect of operating conditions (Section 3) and catalyst properties (Section 4) on selectivity and activity are rationalized, and Table 1 compiles all referenced experiments for easy reference and summarization. We include an analysis of how the bifunctionality of this catalyst can allow for tunability to maximize selectivity of desirable products (Section 5). Finally, we discuss remaining uncertainties and potential future investigations (Section 6).

2. Mechanism

Efforts to understand the interplay between the mechanisms taking place on the nickel and acid sites in Ni-based aluminosilicates remain challenging mainly due to the difficulty in deconvoluting which reactions occurred on which active site. For example, residual acid sites on Ni-supports could also catalyze alkene oligomerization and isomerization reactions [15,23].

Despite these challenges, even early literature deduced that the nickel site was responsible for oligomerization of ethylene to light, linear, even-numbered alkenes by identifying a familiar Schulz-Flory distribution. This was referred to as the *true oligomerization pathway* [14,23,32]. Using homogenous catalyst insight, the Cossee-Arlman and metallacycle-like mechanisms were first postulated for heterogenous Ni-oligomerization (Fig. 2) [1,7,33]. Initial studies assumed the metallacycle was being followed as no co-catalyst is required for the metallacycle but is required for the Cossee-Arlman mechanism. Only from recent experiments [15,34,35], first-principles calculations [36,37], and kinetic modeling [38,39], nearly all studies have concluded that the heterogeneously nickel-catalyzed reactions, including metal-organic frameworks [40,41], follow the Cossee-Arlman mechanism, with the framework acid site helping to form the active Ni site. The latter mechanism is often associated with Ziegler-Natta catalysts, used in the synthesis of 1-alkene polymers. Other homogenous transition metal catalysts such as cobalt, iron, and titanium are believed to follow the Cossee-Arlman mechanism as well [2,41–43].

Generally, the mechanism involves a catalytic cycle that starts with an activation step and continues to subsequent coordination and insertion (chain growth) steps (Fig. 3). A termination step closes the cycle and returns the metal to its active state, while releasing a longer, linear

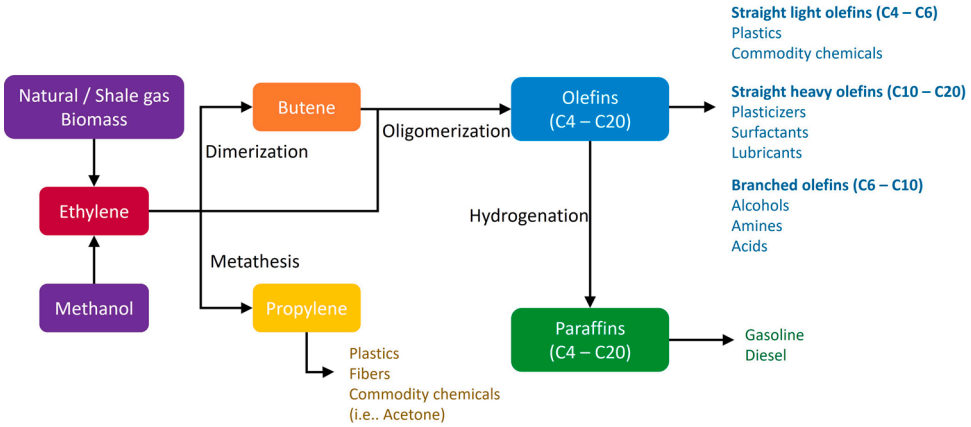

Fig. 1. Ethylene feedstock and major valuable products.

Table 1
Operating conditions and catalytic performance of oligomerization of ethylene on various Ni-acid catalysts.

Ref	Catalyst			Ethylene dimerization & oligomerization									
	Support	Ni (% wt)	Si/Al	Temp (K)	Ethylene Pressure (MPa)	Reaction mode	Rate of ethylene oligomerization	Conversion Ethylene (%)	C4 Selectivity (%)	1-Butene fraction	C6 Selectivity (%)	C8 Selectivity (%)	C10+ Selectivity (%)
[34]	$NiSO_4$-Al_2O_3	2.0		393	2.9	flow	2.5×10^{-5} (mol /g_{cat} s)	10–25	75 - 55	0.12 – 0.25	-[a]	-[a]	-[a]
[34]	$NiSO_4$-SiO_2-Al_2O_3	2.0		393	2.9	flow	2.2×10^{-5} (mol /g_{cat} s)	15–25	75 - 50	0.12 – 0.15	-[a]	-[a]	-[a]
[38]	Ni-SiO_2-Al_2O_3	1.8		443 - 503	0.15 - 0.35	flow	7.0×10^{-6} - 2.7×10^{-5} (mol /g_{cat} s)	4 - 18	2 - 14	0.3 – 0.4	1 - 3	-[a]	-[a]
[22]	Ni-SiO_2-Al_2O_3 (Ni-SA-I)	0.76		393	3.5	fixed-bed flow	-[a]	99	18[b]	-[a]	13[b]	22[b]	41[b]
[56]	Ni-AlSBA-15	2.6	7.0	323 - 573	1.0 - 4.0	flow and batch	4.4×10^{-2} – 4.9×10^{-2} (g_{olig} /g_{cat} s)	15 - 99	41 - 77[b]	0.15 – 0.36	17 - 26[b]	4–21[b]	2–5[b]
[25]	Ni-Y	1.7 – 5.6	1.5 - 3	323 - 343	0.6 - 4.1	flow	-[a]	1.3 - 18.5	51 – 87[b]	0.67–0.80	-[a]	-[a]	-[a]
[23]	Ni-Y	3.7	2.8	388	3.5	flow	1.86×10^{-2} (mol /mol_{Ni} s)	98	46[b]	-[a]	19[b]	16[b]	21[b]
[26]	Ni-Y	0.6 – 1.5	6 - 30	303 - 343	4	semi-batch	2.8×10^{-3} - 8.3×10^{-3} (g_{olig} /g_{cat} s)	-[a]	95–23[b]	0.88 – 0.10	5–10[b]	2–27[b]	1–30[b]
[63]	Ni-ZSM5	0.9	77	523, 723	0.15, 2	fixed-bed	-[a]	95 - 5	12 - 35	0.20 – 0.25	5 - 20	-[a]	0 – 60
[34]	Ni-BEA (micro)	2.2	24.0	393	2.9	flow	2.0×10^{-5} (mol /g_{cat} s)	10–25	60 - 30	0.26 – 0.50	-[a]	-[a]	-[a]
[34]	Ni-BEA (nano)	2.1	17.4	393	2.9	flow	4.0×10^{-5} (mol /g_{cat} s)	10–25	78 - 35	0.25 – 0.47	-[a]	-[a]	-[a]
[4]	Ni-BEA	1.5 - 6.0	12.5	303 - 463	3.5 - 6.5	fixed-bed	-[a]	92–10	45 - 27[b]	-[a]	55–45[b]	5–10[b]	1–2[b]
[14]	Ni-BEA	1.0 - 2.5	12	393	3.5	fixed-bed	-[a]	7 - 75	38 - 72[b]	-[a]	8–13[b]	7–14[b]	2–36[b]
[82]	Ni-BEA	3.4	12	323 - 463	0.9 - 2.6	fixed-bed	-[a]	57 - 38	60 - 85[b]	-[a]	5–13[b]	2–13[b]	2–10[b]
[15]	Ni-BEA	1.1	11	453	4.0×10^{-4}	flow	3.0×10^{-4} (mol /mol_{Ni} s)	1.4	90	0.25	-[a]	-[a]	-[a]
[39]	Ni-BEA	4.9	12.5	443 - 543	0.17 – 0.40	flow	6.0×10^{-6} – 1.8×10^{-5} (mol /g_{cat} s)	10 - 16	90 - 84	-[a]	13–7	-[a]	-[a]
[83]	Ni-BEA	5.2	12	393	0.1 – 2.6	fixed bed	-[a]	0.6 – 91.2	92.8[b]	-[a]	7.2[b]	0–21[b]	-[a]
[84]	Ni-MCM-22	0.55	14	343, 423	4.0	semi-batch	3.1×10^{-4} -6.9×10^{-4} (g_{olig} /g_{cat} s)	-[a]	82	0.1	5 - 7	10 - 13	1
[84]	Ni-MCM-36	0.5	26	343, 423	4.0	semi-batch	1.1×10^{-3} - 2.8×10^{-3} (g_{olig} /g_{cat} s)	-[a]	45 - 81	0.24 – 0.55	8 - 25	6 - 15	5 - 17
[100]	Ni-MCM-41	0.5	10 - 30	473	0.1	semi-batch	1.8×10^{-2} – 2.7×10^{-2} (g_{olig} /g_{cat} s)	-[a]	41–49	-[a]	15 - 35	12 - 24	4 - 20
[63]	Ni-MCM-41	0.7	52	523, 723	0.15, 2	fixed-bed	-[a]	7 - 50	60 - 80	0.30	8 - 24	-[a]	0
[87]	Ni-Al-MCM-41	0.4	36 - 75	423	3.5	batch	1.1×10^{-2} – 2.4×10^{-2} (g_{olig} /g_{cat} s)	-[a]	40–55[b]	0.15 - 0.22	15 - 30[b]	15–25[b]	10–25[b]
[83]	Ni-Al-MCM-41	5.7	13	393	0.1	fixed bed	-[a]	2.82 – 92.2	91.5[b]	-[a]	7.0[b]	1–31[b]	-[a]
[100]	Ni-MCM-48	0.5	30	473	0.1 – 2.6	semi-batch	3.1×10^{-2} (g_{olig} /g_{cat} s)	-[a]	42	-[a]	37	14	7
[62]	Ni-CFA-1	1, 7.5		295	5	semi-batch	0.5–10 (mol / mol_{Ni} s)	-[a]	88 - 97	0.91 - 0.94	2–5	-[a]	-[a]
[59]	Ni-Facac-AIM-NU-1000 & Ni-Acac-AIM-NU-1000	3.5[c]		318	0.2	flow	3.5–4.4 $\times 10^{-2}$ (mol / mol_{Ni} s)	0.5 - 2.5	100	0.8	-[a]	-[a]	-[a]

[a] no number reported.
[b] mass, wt.%.
[c] Ni per Zr_6 no.

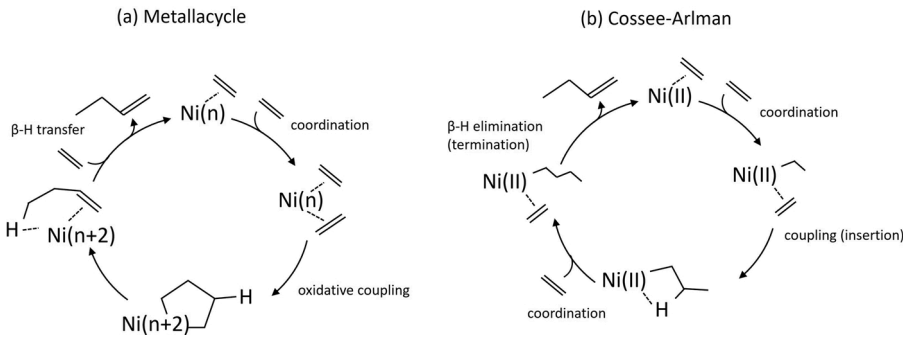

Fig. 2. Simplified schematic of the (a) metallacycle mechanism and (b) Cossee-Arlman (or coordination-insertion) mechanism for ethene dimerization over a Ni active site, based on homogenous catalysis (no charges indicated). In the (a) metallacycle, n and n+2 refer to the oxidation state; for example, in homogenous systems this would be Ti(II)/Ti(IV) or Cr(I)/Cr(III) [44]. In the (b) Cossee-Arlman mechanism the oxidation state remains +2.

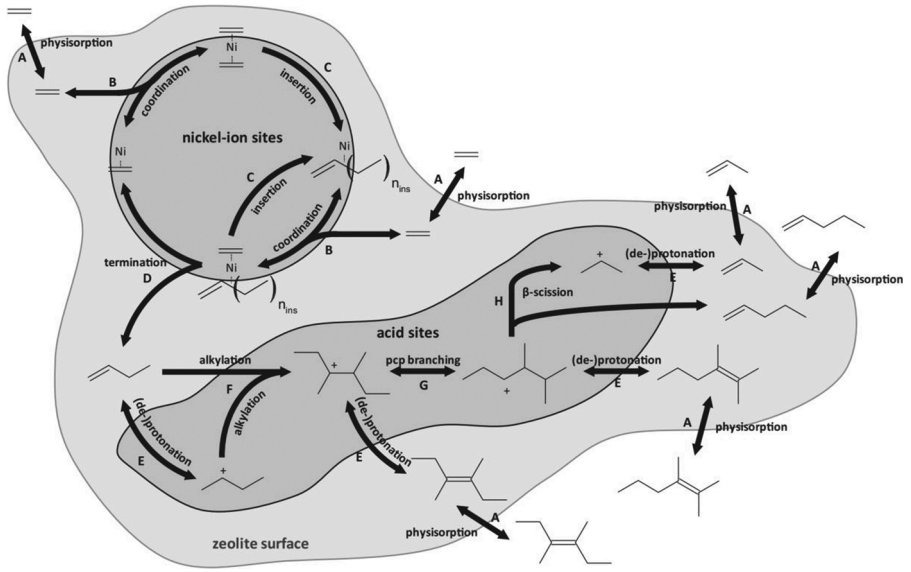

Fig. 3. Schematic representation of the ethylene oligomerization network involving Ni-ion oligomerization and acid-catalyzed alkylation, isomerization and cracking from Toch et al [39].

alkene oligomerization product. This linear alkene can then quickly undergo further acid-catalyzed oligomerization, referred to in early literature as the *hetero-oligomerization pathway,* including isomerization and cracking reactions to produce a variety of products. In the following sections, the focus will be on the detailed mechanisms occurring over each of the active sites.

2.1. Nickel site

The initial Ni site and activation mechanism remain unclear even today. Such difficulty in identifying the actual active sites is mainly the result of various Ni states simultaneously observed by spectroscopy on working catalysts, namely Ni^0, Ni^+, and Ni^{2+}, as well $NiOH^+$. Moreover, the support morphology and Ni incorporation method may greatly affect Ni precursors and the initial activation mechanism of the Ni upon the support [45].

Based on electron paramagnetic resonance (EPR), diffuse reflectance infrared Fourier transform spectroscopy (DRIFTS), and X-ray photoelectron spectroscopy (XPS), Ni^+ has been cited as an influential site, an uncommon oxidation state thought to be formed from partially reduced Ni^{2+}, and perhaps directly involved in the formation of an active nickel site [1,45–47]. Likewise, there have been studies that report Ni^{2+} grafted on acidic frameworks as the active species in Ni-BEA and Ni-MCM-41 under steady state conditions, based on operando CO Fourier-transform infrared spectroscopy (FTIR−CO) experiments [35,48]. While there exists at least one paper published in the past to support any one of these precursor Ni states, the most abundant and recent studies suggest nickel (II) cations in exchange positions to be the active catalytic species as seen in Ni-BEA [14,15,34], Ni-Y [23], Ni-X [49], Ni-MCM-41 [50], and Ni-silica-alumina [22,51] based on FTIR−CO, UV–vis, X-ray absorption near edge structure (XANES), and Ni K-edge X-ray absorption spectroscopies. Additionally, only Ni^{2+}-sites and strong acid sites are needed for heterogeneous catalytic ethylene oligomerization; conversely homogenous nickel catalysts also require an alkylaluminum co-catalyst [7,21,24].

Despite several decades of experimental studies of olefin oligomerization, a clear determination of the nickel active site before ethylene coordination and the start of the oligomerization cycle is yet to be validated beyond doubt [7]. For the point of illustrating a potential activation mechanism, ion exchanged Ni^{2+} structures were assumed as the basis for the active site, though this may vary depending on catalyst synthesis. Activation is proposed to begin from the $[Ni(II)-OH]^+$ species, which has been reported for Ni-silica-alumina (Fig. 4a) [37,52]. Ethylene coordinates to this initial species to form a Ni-vinyl intermediate that has been observed by Moussa et al. [35]. The final active and resting state is an anchored $[ethylene\text{-}Ni(II)\text{-}ethylene]^+$ which is also consistent with Joshi et al.'s adsorption data indicating the resting state to be in a tetrahedral coordination with oxygen in the first coordination

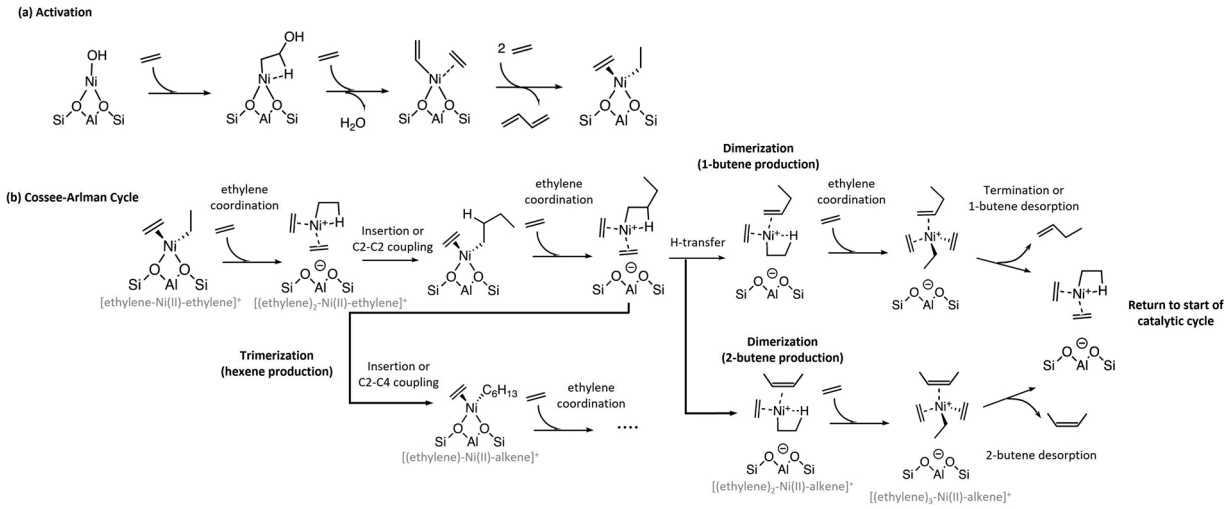

Fig. 4. Reaction mechanism of Cossee-Arlman Ni(II) site by Brogaard et al [37] with a) proposed activation of exchanged-Ni in a mesoporous support, though mechanism may differ slightly based on synthesis method; b) proposed insertion – termination cycle for chain growth (dimerization and trimerization) with isomerization considerations taken from Joshi et al [15]. Charges refer to overall complex charge.

shell [15]. The duration of the transient activation period was shown to decrease with increasing ethylene pressure [15,33]. Joshi et al. concluded that the active Ni^{2+} complex is formed *in situ* upon reacting with ethylene [15]. Additionally, at certain conditions (> 0.6 kPa at 453 K for Ni-BEA), this activation period can be assumed to be instantaneous and irreversible [15,38]. This has been supported by kinetic models made by Toch et al. who found the activation enthalpy quite exothermic and much more negative than the coordination enthalpy. A simplified model in which instantaneous and irreversible activation was assumed did not have a pronounced effect on the residual sum of squares or the statistical significance for the model [38]. These findings suggest that the choice of reaction conditions can determine whether the initiation steps are fast enough to avoid detection.

Joshi et al. [15], Henry et al. [34], and Moussa et al. [35] provided experimental confirmation that Ni follows the Cossee-Arlman mechanism, rather than the metallacycle, in 2018. By comparing the Ni oxidation state, intermediate site geometry, and product selectivity, summarized in Table 2, Joshi et al. concluded the Cossee-Arlman mechanism behavior was dominating. A Ni^{2+} oxidation state was concluded based on CO IR peaks at 2213 and 2206 cm^{-1} for $Ni^{2+}(CO)$ and $Ni^{2+}(CO)_2$ complexes, respectively. Henry et al. (peaks at 2212 and 2202 cm^{-1}) and Moussa et al. (peaks at 2214 and 2205 cm^{-1}) drew a similar conclusion from CO IR spectroscopy and adsorption studies that ethylene reacts with a Ni^{2+} ions to form Cossee-Arlman oligomerization sites [34,35]. The first energetic calculations to understand ethylene oligomerization on nickel in a zeolite were done by Brogaard and Olsbye in 2016 [36]. These energetic studies using AFI topology suggested that ethylene dimerization to 1-butene on nickel followed the more energetically favorable Cossee-Arlman mechanism, not the metallacycle (see Table 2). Brogaard et al. revisited this mechanism proposing that the Ni^{2+} exists as both a mobile and an anchored complex during the dimerization mechanism [37]. This is in line with recent studies that also revealed the active site in heterogeneous catalysts to be mobile [53–55]. The highly-complexed mobile active site is consistent with Joshi et al.'s EXAFS regions that show Ni-O coordination numbers corresponding to tetrahedral Ni^{2+} cations.

Table 2
Comparisons between Cossee-Arlman (or coordination-insertion) and metallacycle mechanisms for ethylene dimerization on Ni complexes [15].

Comparison	Analysis	Cossee-Arlman	Metallacycle
Initial active site	H/D isotopic scrambling, H_2-D_2 exchange	$[Ni(II)-H]^+$	Ni(n)
Ni oxidation state	CO IR, DRUV, *in situ* XAS spectroscopy	+2	n, n+2
Intermediate geometry	DRUV, XANES, EXAFS	four-coordinate, distorted tetrahedral complex	metallacyclopentane complex
Product selectivity	Oligomerization experiments	1-butene cis and trans-2-butene	1-butene
Estimated energy span	DFT	71 kJ/mol[a]	171 kJ/mol[a]

[a] Ref [36].

In comparison to the Cossee-Arlman investigations, there have been only a few experimental studies [56] and DFT studies [57] focused on the metallacycle mechanism, but these studies do not compare against the possibility of the Cossee-Arlman mechanism. There has been no inference of a Ni-metallacyclopentene intermediate reported in heterogenous literature. The metallacycle is often assumed on the basis that no co-catalyst is required for heterogeneous Ni-oligomerization; in homogenous catalysis the metallacycle needs no co-catalyst, while the Cossee-Arlman mechanism does. However, heterogeneous active sites are likely formed with the help of framework acid sites, as discussed earlier in the section, and this better understanding now points the oligomerization towards the Cossee-Arlman mechanism.

Although active site formation may be nuanced to the catalyst's Ni-incorporation method or framework support, ethylene oligomerization likely proceeds through the Cossee-Arlman mechanism despite these differences, as the mechanism has been confirmed on a variety of heterogenous supports as well as Ni-MOFs [40,58,59]. Throughout the mechanism, it is believed the Ni species can exchange between the oxygen atoms of the zeolite and ethylene, to reversibly switch between an anchored and mobile complex [37]. After activation, Ni predominately maintains a constant formal +2 oxidation state throughout chain growth reactions via the Cossee-Arlman cycle (Fig. 4b) [15,34,36,49]. Brogaard et al. compared the energies among $[ethylene-Ni(II)-ethylene]^+$, $[(ethylene)_2-Ni(II)-ethylene]^+$, and $[(ethylene)_3-Ni(II)-ethylene]^+$ complexes, where Ni is coordinated with two, three, and four ethylene molecules, respectively, to find the most likely insertion-termination mechanism. The anchored $[alkene-Ni(II)-alkene]^+$ complexes are affixed by two Ni-O bonds to the framework. The mobile $[(alkene)_2-Ni(II)-alkene]^+$ and $[(alkene)_3-Ni(II)-alkene]^+$ complexes mimic a homogenous oligomerization catalyst in solution, but the positively charged complex still remains tethered to the zeolite framework by the

Table 3
Catalytic characteristics and behavior of Ni-exchanged ethylene oligomerization at 423 K in semi-batch reactor.

Ref	Catalyst	Ni (wt. %)	Si/Al	BET surface area (m^2/g) (external)	Main pore system	Acid amount (mmol NH_3/g)	Average activity (g_{oligo}/g_{cat} h)	Product distribution (% mol)			
								$C_4^=$	$C_6^=$	$C_8^=$	$C_{10+}^=$
[84]	Ni-MCM-22	0.55	14	110	micro	0.95	2.5	81	5	13	1
[84]	Ni-MCM-36 (1)	0.5	26	800	micro + meso	0.65	39	54	15	15	17
[84]	Ni-MCM-36 (2)	0.6	26	800	micro + meso	0.70	46	45	25	15	15
[100]	Ni-MCM-41 (1)	0.5	10	820	meso	0.70	64	41	15	24	20
[100]	Ni-MCM-41 (2)	0.5	20	930	meso	0.60	72	45	19	21	15
[100]	Ni-MCM-41 (3)	0.5	30	1000	meso	0.45	88	49	35	12	4
[100]	Ni-MCM-41 (4)	0.5	30	1300	meso	0.45	97	48	33	14	5
[100]	Ni-MCM-48	0.5	30	1070	meso	0.44	113	42	37	14	7

negative ion-exchange site [37,60]. Three- and four-coordinated Ni^{2+} ions were also observed by Tanaka et al. through Fourier transform infrared (FT-IR) and X-ray absorption fine structure (XAFS) spectroscopy as well as Joshi et al. via EXAFS data [15,50]. Joshi et al. also notes a $[Ni(II)\text{-}H]^+$ active intermediate also proposed within Brogaard et al.'s most recent DFT-based mechanism, $[(ethylene)_2\text{-}Ni(II)\text{-}ethylene]^+$, that allows for the mobile Ni species to achieve its preferred square-planar coordination [37,61]. This type of $[Ni(II)\text{-}H]^+$ or $[(ethylene)_2\text{-}Ni(II)\text{-}alkene]^+$ species is also referred to as a *beta agostic* complex. The consecutive coordination and insertion of $[(ethylene)_2\text{-}Ni(II)\text{-}alkene]^+$ *beta agostic* complexes allow for chain growth to form complexed butenes, hexenes, etc., or the $[(ethylene)_2\text{-}Ni(II)\text{-}alkene]^+$ can coordinate with ethylene and terminate to release the coordinated alkene and return the Ni to the activated complex. In homogenous nickel systems that also follow a Cossee-Arlman-type mechanism, the insertion of the olefin was often found to be a rate-determining step [7].

Notably, Ni^{2+} Cossee-Arlman sites have been shown to produce both linear 1- and 2-butenes in non-equilibrated ratios, indicating primary butene double-bond isomerization events via the Ni^{2+} site [15,24,52]. In some previous studies, 2-butene was thought to be a secondary product from solely acid sites [15,33,34]. However, even homogeneous nickel catalysts with proper ligands ($NiCl_2(PBu_3)_2$) can orient the selectivity toward 2-butenes; by comparison, it is very likely such a pathway exists for heterogeneous nickel catalysts [7]. Lallemand et al. studied butene fractions using NiY and found that the proportion of 1-butene decreased rapidly with increasing temperature from 276 K to 343 K. Yet, these results are likely mixed with the effect of acid-site isomerization. Nevertheless, at low temperatures, of the C4s produced by NiY, 80 % were 1-butenes [24,26]. MOFs have been able to almost exclusively (88–99 % selectivity) produce 1-butenes in the proper environment [59,62]. Joshi et al. and Henry et al. both further investigate 1-butene/2-butene ratios on heterogenous Ni-supported catalyst with minimal acidity at 453 K and 393 K, respectively. Both find a high initial formation of 2-butene, suggesting the 2-butene production pathway is initially kinetically favored by nickel (1-butene fraction ~20 – 50 % of all C4s) at these temperatures [15,34]. Brogaard et al. found 1-butene selectivity doubled at constant conversion when increasing the ethylene pressure from 0.4 MPa to 1.8 MPa (408–438 K), suggesting that at high ethylene pressures, ethylene can more easily replace 1-butene before isomerization, limiting 2-butene formation on Ni sites [37]. Joshi et al. proposed an isomerization pathway that has been slightly adapted to fit into Brogaard et al.'s Cossee-Arlman mechanism (Fig. 4b) [15,37]. Beyond conditions of low conversion and low acidity, it is difficult to tell which site is responsible for internal isomerization as both sites are capable of such chemistry.

The nickel site's Cossee-Arlman mechanism discussed above produces a statistical Schulz-Flory product distribution (Fig. 5) [1,2,23,34,38]. A Schulz-Flory distribution remains at the heart of many commercial higher olefin production processes, such as Ziegler-Natta catalysis used by INEOS, Chevron, BP, and DuPont, to name a few [2]. This distribution can be summarized by a chain growth probability α : the probability that a growing oligomer chain will propagate, or insert, rather than terminate. Lower values of α will tend to terminate over insert, leading to lighter products, in this case butene. Conversely, higher α values favor insertion, producing heavier products. For a given α, the mole fraction (x_n) and the carbon selectivity ($S_{C,n}$) of an oligomer consisting of n monomer units can be calculated with Eq. 1 and Eq. 2, respectively [2]. Operating conditions can change the value of α. Heveling et al. found that the growth factor α increased with nickel loading (1−4 wt.%) on Ni-Y at 423 K from about 0.1 – 0.5 [23]. Additionally, nickel content can change the value of alpha. For catalysts with a lower nickel content, a plateau of a maximum alpha value (~ 0.1 – 0.3) was reached with increasing conversion. For catalyst with a higher nickel content that were highly active, it appeared that the highest alpha values (~ 0.5) corresponded to almost total feed consumption, and the reaction ceased before a plateau was reached. Thus, it is highly likely that the alkenes in the Ni-complexes, such as $[alkene\text{-}Ni(II)\text{-}alkene]^+$, will be

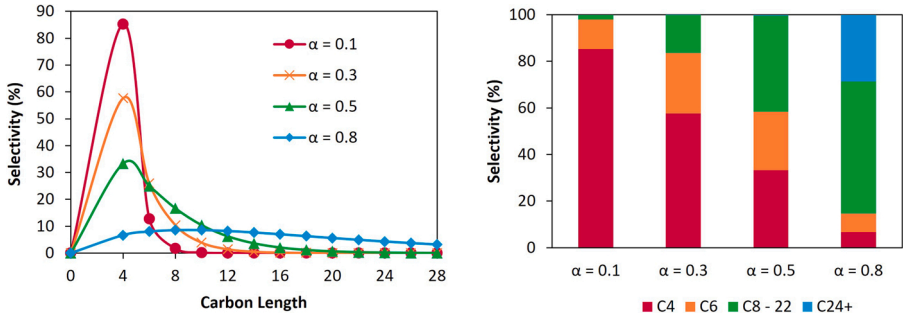

Fig. 5. Schulz-Flory product distribution for ethylene oligomerization at various chain-growth probabilities (α).

ethylene or butene, and to a lesser extent hexene or octenes.

$$x_n = (1-\alpha)\alpha^{n-1} \quad (1)$$

$$S_{C,n} = \frac{\left(n(1-\alpha)^2\alpha^{n-2}\right)}{2-\alpha} \quad (2)$$

Other reactions have been hypothesized to occur on the Ni site in addition to those discussed above. The Ni site has been proposed, at significantly high temperatures, to also catalyze dehydrogenation reactions to convert cycloalkenes into aromatics [63]. However, currently no detailed study that confirms this reaction has been published. Rather, it may be possible that loaded nickel oxide was reduced to metal, which acts as a dehydrogenation active site during the aromatization process [64]. Direct conversion of ethylene to propene using Ni-MCM-41 catalysts has also been explored. A few labs have suggested that a Ni-metathesis reaction in the phyllosilicate structure may occur at sufficiently high temperatures (> ~673 K) [65–68]. But more recently in 2017, there was evidence of conjunct polymerization products that can be cracked down to propene as a more plausible route and more in line with our current understanding of the mechanism [69,70]. This has also been supported by kinetic modeling on Ni-MCM-41, where a reaction network based on the cracking of long-chain olefins better fit and predicted the observed product distributions than a network containing metathesis reactions [71]. Additional mechanistic uncertainties are reviewed in Section 6.2.

2.2. Brønsted acid site

Hydrocarbon oligomerization on Brønsted acid sites has been well studied in the past, and the reaction families are generally well known: alkylation, isomerization (hydride shift, methyl shift, protonated cyclopropane (PCP) branching), and β-scission reactions, see Fig. 6 [1,3–5,15,34,63]. These are preceded and followed by chemisorption of the alkene reactants and products via protonation and deprotonation, respectively. At sufficiently high temperatures (> ~600 K), hydride and alkyl transfer can result in alkane products [72]. Long-chain oligomerization, cyclization, as well as aromatization reactions can lead to coke formation at high temperatures as well. Generally, oligomerization reactions are the most important acid-catalyzed steps for lower carbon number species. C8+ species more often undergo isomerization and cracking reactions involving more stable (tertiary) carbenium ions, producing branched, internal alkenes of even or odd carbon numbered hydrocarbons [4,39].

At intense reaction conditions (e.g., high temperature, > ~500 K) acid catalysts alone can oligomerize ethene. In many Ni/acid catalyst studies, the acid support precursor is often run at the same conditions as the Ni-containing catalyst for comparison, as was done for H-BEA by Joshi et al. [15] and Henry et al. [34], and H-ZSM5 by Jin et al. [63]. At these intense reaction conditions, the product distributions from solely acidic zeolites include a variety of linear and branched alkenes and alkanes from acid-catalyzed alkylation, cracking, and isomerization reactions. Reactions via secondary and tertiary carbenium ions can be considered to occur whenever acidity is sufficiently pronounced. At very high acid strengths and high temperatures, primary carbenium ions can start contributing to an applicable extent [73,74]. Carbenium ions formed on acid sites will prefer to rearrange via more stable secondary and tertiary carbenium ions to form internal alkenes and branched products [72]. For C4 alkenes, this often will take the form of isobutene. Because acid sites can produce isobutene via acid-catalyzed alkylation and cracking, while the Ni site can only produce linear butenes via insertion-growth mechanisms, isobutene is often used as an indicator of residual acid chemistry in experimental studies [15,34].

2.3. Across nickel - brønsted sites

An analysis of the branching degree can provide valuable insight into the type of oligomerization events occurring on a catalyst, although it is rare for a study to report such detailed breakdowns. Interestingly, Martinez et al., Lallemand et al., and Andrei et al. analyze the branching degree and find products of predominately linear butenes, linear hexenes, and branched octenes [14,26,56]. These results point towards Ni-catalyzed oligomerization to create up to linear ethylene trimers, and higher oligomers are then formed via acid-catalyzed reactions involving C4 and C6 alkenes, in line with their affinity towards more highly branched products.

At low conversion, it is generally believed that ethylene will first interact with the nickel site to dimerize or trimerize yielding linear alkenes which then interact with the acid site for further reactions. This sequential behavior was the underlying logic in Toch et al.'s SEMK model and has also been postulated in Hulea's review [6,39]. At high conversion when ethylene concentrations are lower, it is entirely possible species larger that ethylene can interact a second time with a nickel site, or co-dimerize, as there have been studies of propylene and butene dimerization on heterogenous nickel catalysts [33,75,76]. Deconvoluting on which site further dimerization occurs at high conversion is challenging as both sites are capable of such chemistry. Once again, branching can provide further insight: monobranched species (e.g. methylheptenes) are favored in metallic codimerization and dibranched species (e.g. dimethylhexenes) are favored in acidic oligomerization [7,12,75]. Unfortunately, literature often reports selectivities by carbon number and are not further refined by degree of branching.

Some of the studies that investigate the Ni/acid mechanism also reported the alkene partial reaction order. This reaction order appears not to be a consistent value, but dependent on the three-dimensional structure of the support. The reaction order in ethylene for butene formation was found to be about first order in alkene pressure on mesoporous Ni-silica-alumina [17,38,77,78]. However, in microporous Ni-zeolites, the ethylene reaction order has been published as first order [15,32,79] as well as second order [34,50,75,80]. Experimental results by Toch et al. concluded there is a first order dependency of the reaction rate on ethylene inlet partial pressure for Ni-SiO_2-Al_2O_3 for

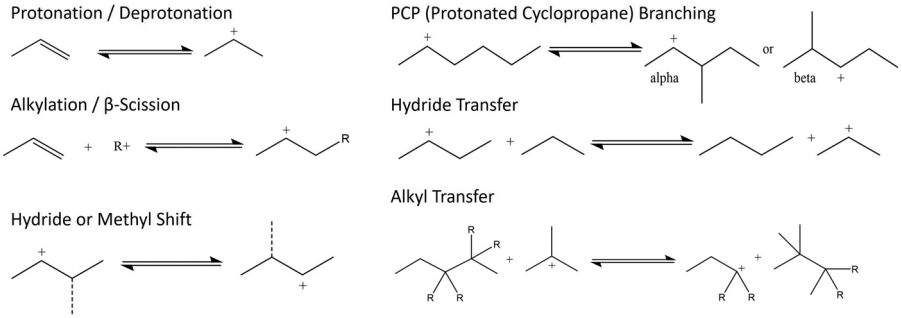

Fig. 6. Acid-catalyzed reaction families based on carbenium ion intermediates with typical reactions shown.

dimerization. Henry et al. tabulated the reaction order in ethene for butene formation to be 1.5–1.7 on mesoporous $NiSO_4$-Al_2O_3 and $NiSO_4$-SiO_2-Al_2O_3, and 2.0 on microporous Ni-BEA. Mlinar et al. found the rate of propene dimerization to be first order in microporous Ni-Na-X [49]. Brogaard et al. observed the rate of butene is second order in ethylene pressure on microporous Ni-SSZ-24 zeolite [37]. Interestingly, second order was only obtained in the group's kinetic model when $[ethyl\text{-}Ni\text{-}alkene]^+$ was the most abundant species adsorbate. The framework might not be the only thing effecting reaction order. Nickel dimerizing larger alkenes than ethylene, pore saturation, or coverage effects may also be contributing, and the discrepancies are further discussed in Section 6.2.

3. Operating conditions

The overall Ni-acid mechanism described in Section 2 can be used to explain the trends in experimental data, many of which Hulea and co-workers [1] and Ghashghaee [28] also cover. Ethylene oligomerization over Ni-acid heterogenous catalysts has been carried out over a wide range of temperatures and pressures and in different reactor types (see Table 1 for the sake of visibility). The distribution of the product oligomers not only depends on the concentration of nickel and acid sites, but also the operating conditions can direct products from dimers to long-chain oligomers, as will be discussed in this section.

3.1. Effect of conversion on selectivity

Fig. 7 shows the evolution of the product selectivity as a function of conversion. At low conversions, ethylene dimerization to linear butene on the Ni-ion site dominates, being the initial combination of steps in the reaction network (also see Fig. 2). With increasing ethylene conversion (by increasing the space-time and decreasing space velocities), ethylene has more time to adsorb onto the catalyst surface and can readily undergo oligomerization or isomerization surface reactions as well as re-adsorption of products to form bulky oligomeric chains. The acid sites contribute more and more to the product formation, resulting in branched octenes. These octenes can be rapidly cracked to form products such as propene, pentene, and isobutene, shifting the (linear) alkene composition [39]. By increasing the ethylene conversion further, the overall butene selectivity decreases in favor of hexenes and octenes [33]. At very high conversions, the acid-catalyzed steps have sufficiently high enough rates to produce a wide and complex product distribution comprising many isomers, reminiscent of a purely acidic zeolite product distribution. Extremely low space velocities and, correspondingly, close to full conversion can cause excessive oligomerization, quickly reducing

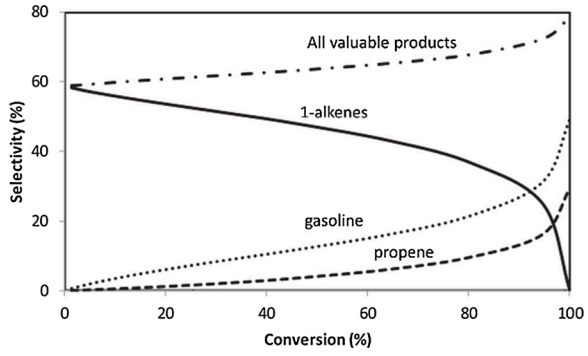

Fig. 7. Selectivity towards valuable product fractions as function of ethylene conversion from Toch et al. on 4.9 wt.% Ni-BEA at 503 K and ethylene inlet partial pressure (= total pressure) of 1.0 MPa. Solid line: linear 1-alkenes; dotted line: gasoline; dashed line: propene; dashed-dotted line: selectivity towards all valuable products (1-alkene + gasoline + propene) Toch et al. excluded some components, such as isobutene, which are instead considered 'losses' [39].

product yields and deactivating the catalyst [81].

Experiments done by Ng et al. on Ni-Y support this paradigm [24]. At mild conditions and lower conversions, the majority of products were butenes and hexenes (51–87 wt.%). At higher conversions, 1-butene selectivity decreased and fractions of C8 – C14 were produced. No odd-numbered alkenes were present, indicating acid-catalyzed cracking reactions did not occur at these reaction conditions (see Table 3 for reaction conditions). Jan et al. also performed oligomerization trials on Ni-BEA by varying space velocity and, hence, ethylene conversion [82]. The steady-state ethylene conversion increased from 44 % to 57 % as space velocity decreased or residence time increased. The increase in conversion was also associated with a decreasing C4 selectivity and an increasing C6, C8, and C10 selectivity. Moussa et al. ran Ni-BEA and Ni-Al-MCM-41 catalysts at high and low conversion; at low conversion (1%) the butene weight fraction dominated (92 wt.%), followed by hexenes (7 wt.%) with very little octene and almost no detectable odd-numbered carbons [83]. At high conversion (90 %), the butene fraction declined to favor gasoline and diesel, with the C8 wt.% climbing to 20−30 wt.%. A similar trend was found by Andrei et al. on Ni-AlSBA-15 [56]. Additionally, Jan et al. found that changing the space velocity from 3.1–5.5 $g_{eth}\ g_{cat}^{-1}\ h^{-1}$ did not significantly affect the transport rate of ethylene from the bulk to the catalyst surface, but does affect the conversion of butene into higher oligomers at the tested conditions [82].

3.2. Time-On-Stream (and deactivation) behavior

Catalyst deactivation with time appears to highly depend on the reaction conditions and the catalyst properties, which will be addressed in each topic of Section 4. In early studies, catalysts based on Ni dispersed on purely microporous zeolites such as X [76], Y [26], and MCM-22 [84] exhibited fast deactivation due to the accumulation of heavy oligomers in the channels and cages. This has been verified by characterizing spent catalysts and finding carbonaceous deposits inside catalyst pores [13,26,58,75]. Similarly, Agirrezabal-Telleria and Iglesias studied ethylene, propene, and butene dimerization and found deactivation to be much faster for larger alkenes [48]. Espinoza et al. used a ~0.2 wt.% nickel-exchanged silica-alumina catalyst at 573 K, 1.15 MPa and reported rather pronounced deactivation, with an initial conversion of about 60 % before dropping to about 20 % after 120 h [17]. Andrei et al. found the quantities of heavy products entrapped in the pores of the catalyst was greater during the first hour of reaction, corresponding to the greater deactivation at the start of the oligomerization test [85]. Throughout experiments done by Joshi et al. on ~1.3 wt.% Ni-BEA at 453 K, it was noted that the catalyst had to be regenerated due to deactivation [15]. Therefore, collecting good kinetic and deactivation data can be difficult depending on time scales; the flowrate must stabilize, and mass transfer effects must be fast enough for intrinsic kinetics to be collected.

Long-time runs appear to be most successful at low temperatures (< 400 K). Heydenrych et al. used a 1.6 wt.% nickel-exchanged silica-alumina catalyst at 393 K, 3.5 MPa and found very little deactivation during experimental runs lasting 900 h with conversion being maintained over 90 % [78]. Similarly, Heveling et al.'s Ni-exchanged silica-alumnia catalyst exhibited high stability and high conversion at 3.5 MPa and 381 K after 108 days on-stream [22]. Martinez et al. ran 1.0–2.5 wt.% Ni-BEA at 393 K, 3.5 MPa and did not observe signs of deactivation for 9 h for the full range of compositions [14]. The steady-state ethylene conversion did depend on the nickel loading and ranged from 5% for the 1.0 wt.% Ni to 80 % for the 2.5 wt.% Ni.

Jan et al. observed the typical drop in activity over the course of the initial 3 h for 3.4 wt.% Ni-BEA at 393 K, 1.9 bar [82]. Afterwards, the ethylene conversion did not diminish much during the remaining 78 h on stream and approached a steady state plateau of about 50 %. Compared to the group's shorter 6 h runs using the same mass of catalyst, the same amount of coke was collected (~8 g), and the selectivities

of odd carbon products did not change significantly, suggesting no additional coke is made after reaching a steady-state. This corresponds to coke yields for the short and long-time runs of 0.07 and 5.4 wt %, respectively, due to the largely different mass of ethylene fed during the two runs. After 8 h, the selectivity of C4 dropped off while C6, C8, and C10 rose, and remained the same for the duration of the run. It may be that at this point, the smaller pores of the catalyst are saturated, such that only large pores remain active and contribute to the reaction; this is similar to how mesoporous catalysts promote the production of higher molecular weight compounds in comparison to microporous supports (see Section 4.5 for effects of pore size) [1,82,84]. Overall, deactivation is suggested to occur due to the buildup of large oligomeric products in pores, which can be mitigated by balancing operating conditions and catalyst properties.

However, there is some evidence that deactivation is more nuanced. An early study using Ni-SiO_2-Al_2O_3 at 473 K and 0.1−0.79 MPa by Kiessling et al. found that propene led mainly to dimers while ethylene produced higher oligomers [77]. He points to this as a sign of different deactivation mechanisms depending on the size of the species. Likewise, the presence of various Ni states, such as reduced Ni^+ or NiOH (as discussed in Section 2.1), could be significant not in the activation mechanism, but rather in the deactivation mechanism [47].

Along these lines, if we expand our scope to look at propene oligomerization, Mlinar et al. has studied activation and deactivation on nickel-exchanged zeolites and aluminosilicates [49,86]. The authors report that all investigated catalysts deactivated with time on stream, but the rate and extent of deactivation depended on geometry and Ni loading. Generally, catalysts with lower Ni loading remained the most active with time on stream, and Ni loading below 0.6 wt.% did not deactivate significantly within 90 min of time on stream after peak activity. Interestingly, high Ni-loading deactivation has been suggested but it also still requires solid evidence [58]. While studying propylene oligomerization on Ni-X, Mlinar et al. showed enhanced deactivation at high Ni loadings and more stable dimerization activity at low Ni loadings. In a Ni-X zeolite the activity decreased hyperbolically with time-on-stream suggesting a two-site deactivation mechanism. Mlinar et al. proposed deactivation at high Ni loading is occurring via a reaction of two nearby Ni-olefin complexes which lead to deactivation of both sites, rather than the formation of large oligomer products as previously suggested [49]. In a following paper, Mlinar et al. found activity decreased exponentially with time-on-stream for Ni-MCM-41of similar Ni loading, suggesting a one-site mechanism likely caused by oligomer blockage [86]. From these studies, high nickel-loading deactivation may be caused by oligomer blockage (exponential deactivation) in mesoporous catalysts like Ni-MCM-41, and by neighboring nickel interactions (hyperbolic deactivation) in microporous catalysts like Ni-X. Deactivation investigations beyond large oligomer blockage are required for a better understanding, as is also mentioned in Section 6.2.

3.3. Temperature effect

Fig. 8 shows the simulated temperature effect on product selectivity. Below about 500 K, a nickel-free acid catalyst is inactive towards ethylene oligomerization [22,84,87,88]. Correspondingly, in this lower temperature range, mainly linear alkenes are produced via ethylene dimerization on Ni-ion sites. As temperature increases, the relative importance of the acid site increases and results not only in longer, but also branched, cracked, saturated, unsaturated, and oligomerized hydrocarbons. Based purely on reaction kinetics, as temperature increases, reaction rates and conversion are also expected to increase.

Jin et al. in 2019 experimentally reported the temperature effect in ethylene oligomerization on Ni-ZSM5 at 523 K, 2 MPa and 723 K, 0.15 MPa (Fig. 9) [63]. At lower temperatures (523 K), the main products were linear butenes followed by hexene, ~66 % and 20 %, respectively, with a near Schulz-Flory distribution with small amounts of pentene and propene. No alkane and aromatic hydrocarbons were generated on the

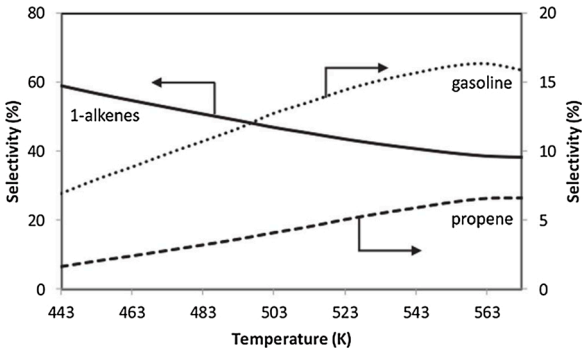

Fig. 8. Selectivity towards valuable product fractions as a function of temperature from Toch et al. at constant ethylene conversion of 50 % and ethylene inlet partial pressure (= total pressure) of 1.0 MPa on Ni-BEA [39]. Solid line: linear 1-alkenes; dotted line: gasoline; dashed line: propene.

Ni-exchanged catalyst. At higher temperatures (723 K) the products spanned a broad distribution of C2 – C6 alkenes, alkanes, and aromatics, indicating that now hydride transfer and cyclization occur at strong acid sites. Some of the other catalysts in this study by Jin et al. also exhibited a decrease in conversion with temperature likely due to coking products and deactivation [63]. Many hypothesize that higher temperatures increase the conversion and activity until coke covers much of the catalyst surface, after which no further increase in the conversion with the temperature is observed [4,63].

Various other experimental studies on different supports such as nickel/sulfated alumina [79], Ni-AlSBA-15 [56], Ni-MCM-41 [63,87], Ni-MCM-36 [84], Ni-Y [88], and Ni-BEA [14] also report largely C4 products at lower temperatures and a much larger variety of C6 – C8(+) products at higher temperatures. At less extreme temperatures than those examined by Jin et al., Andrei et al. compared Ni-AlSBA-15 at 323 K–573 K and found not only did conversion increase strongly, but also the C4 products were directed towards to formation of C6 and C8 as temperatures increased [56].

3.4. Total pressure effect

There did not appear to be a consistent relationship between increasing pressure and light alkene selectivity, likely due to the complexity of the reaction network and to the challenge of decoupling pressure effects from deactivation and conversion. Experimental studies often do not report various pressure runs while keeping conversion constant nor do they discuss pressure effects to the same extent as temperature or catalyst properties. Additionally, the composition of the catalyst, type of the reactor, and time during evaluation could cause further perplexity.

Jan et al. analyzed ethylene oligomerization over Ni-BEA at 393 K at 0.85, 1.90, and 2.56 MPa [4]. The authors reason that at high pressure and high concentrations of ethylene, ethylene can more readily adsorb onto Ni and acid sites, contributing to a higher overall ethylene conversion. Contrarily, lower pressures will increase the likelihood that ethylene could pass through the system without interacting with an active site due to lower surface coverage. Therefore, as the pressure increased from 0.85 to 1.90 MPa, the C4 species has a higher likelihood of interacting with an active site and producing more C6, C8, and C10 species. Further increasing the pressure from 1.90 to 2.56 MPa may encourage species to reabsorb onto the catalyst to form even larger molecules, such as coke. In addition, Nicolaides et al. found that the 1-hexene selectivity was the highest at an intermediate pressure (1.5 MPa in a range of 1.0–3.5 MPa) [89]. This is expected for a mechanism capable of producing C4 – C8 products. For thermodynamic reasons, lower pressures favor smaller species such as C4, while higher pressures will favor larger species (C8); an intermediate pressure should favor an intermediate product such as C6.

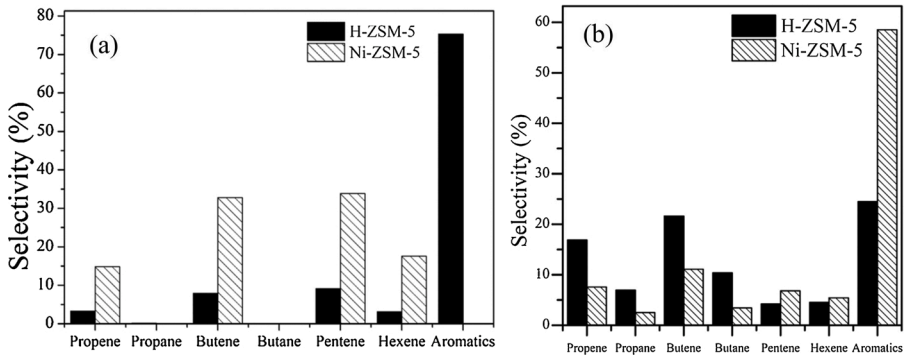

Fig. 9. The distribution of major products of H-ZSM-5 and Ni-ZSM-5(0.7) at a) 523 K, 2 MPa and b) 723 K, 0.15 MPa [63].

In Jan et al.'s studies, coke yield, which can be correlated to deactivation, and initial catalytic activity appeared to linearly increase with ethylene partial pressure. Hulea and Fajula found this linear trend on Ni-MCM-41; Andrei et al. on Ni-AlSBA-15 [56]; Nicolaides et al. on Ni-alumina-silica; and Ng and Creaser on Ni-Y [24,25,87,89]. Hulea and Fajula consider this behavior to be principally due to ethylene solubility dependence on pressure [87]. Reaction rates, especially reactions such as coordination in which ethene is a reactant, would also be expected to increase with increasing pressure. Likewise, thermodynamics may again play a role by pushing products to larger species at higher pressures and more quickly making coking products, as coke formation is largely a bimolecular reaction.

4. Catalyst properties

4.1. Effect of acid sites

In the acidic framework support, carbenium ions are formed by reaction with a proton donated by a Brønsted acid site. Fig. 10 shows the effect of the 'acid site strength' and their concentration on the product selectivity. 'Acid site strength' is expressed as the alkene standard protonation enthalpy – the more negative the protonation enthalpy, the stronger the acid (Fig. 10a). At relatively weak acid sites, the catalyst mimics a purely Ni catalyst and produces mainly linear 1-alkenes with a near-Schulz-Flory distribution. With a more negative protonation enthalpy or growing acid strength, these linear alkenes are more easily transformed into heavier, branched and cracked products [39].

While acid site strength has an exponential effect on the isomerization and cracking rates, acid site concentration has a proportional effect. Changing the ratio of Ni^{2+} / H^{+} within the zeolite is not likely to result in as dramatic a change as the acid site strength (Fig. 10b). While acid strength affects the rates in an exponential manner, Ni and acid site concentration affects rates proportionally. On the other hand, the latter can be more straightforwardly manipulated, and even precisely controlled, when synthetizing the catalyst and/or the support. Note that a very high acid site density is detrimental to the activity of the catalyst by promoting formation of pore-blocking large oligomers and leading to fast deactivation [1,51,87].

Espinoza et al. investigated silica-alumina catalysts with various amounts of nickel-exchange and found product weight increased with increasing acid strength [17]. Lallemand et al. commented on acid site density effects by varying the extent of dealumination in Ni-Y zeolites [84]. A too high density resulted in the formation of long-chain oligomers that blocked pores. A too low density resulted in a product spectrum dominated by butenes and some hexenes, which could be undesirable if the goal is fuel-range products. Moussa et al. studied Ni-BEA and Ni-Al-MCM-41 with similar nickel content but difference acid density [83]. At about 90 % conversion, the higher acid containing Ni-BEA produced 90 wt.% of C8 product compared to 80 wt.% from Ni-Al-MCM-41. Additionally, the C8 fraction obtained on the former, more acidic catalyst, contained more di-branched (80 wt.% di-branched, 20 wt.% mono-branched) than that obtained over the latter, less acidic catalyst (70 wt.% di-branched, 30 wt.% mono-branched), suggesting acid provokes further oligomerization. Lu et al. adjusted the acidity of Ni-MCM-22 through organic alkaline treatment, decreasing the Si/Al ratio to increase the amount of weak acid sites at the expense of strong acid sites [64]. The slight decrease in acidity appeared to enhance the alkylation of light alkenes or inhibit the β-scission of heavier alkenes; the production shifted to favor C6 and C7 olefins over propene and aromatic compounds.

Wang et al. used the desorption activation energy (DAE) of ammonia as a measure for 'acid site strength' to quantify the relationship between acidity and activity for ethylene oligomerization on Ni-MCM-41 [90]. The group used an adapted Brønsted equation for homogenous acid-catalyzed reactions to back out parameters for a model that predicts activity changes with acid site strength. The group found linear trends

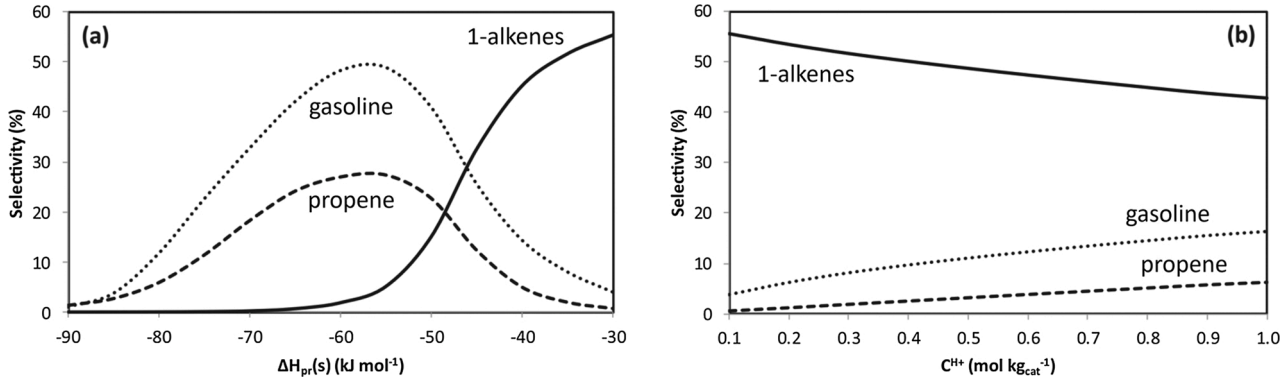

Fig. 10. Selectivity towards valuable product fractions as function of (a) alkene standard protonation enthalpy and (b) acid concentration from Toch et al. at constant ethene conversion 50 %, 503 K, ethylene inlet partial pressure (= total pressure) of 1.0 MPa on Ni-BEA. [39].

between experimental activity and production of different products (e.g. conversion, 1-butene, 2-butene…) against total acid amount. This is similar to what Toch et al. reports in Fig. 10b as a function of the acid site concentration.

4.2. Effect of nickel sites

The effect of ethylene coordination enthalpy and nickel content is opposite to that of acid site strength and concentration. A Ni-acid catalyst with a more exothermic coordination enthalpy or a higher nickel content will have an increased impact of Ni-ion on the product formation, mainly resulting in a higher ethylene conversion and more particularly production of light, linear alkenes (mostly butenes), which can feed into acid catalysis.

Espinoza et al. found increasing the nickel content on Ni-exchanged silica-alumina increased the production of lighter products, but also enhanced deactivation [17]. Heveling et al. performed ethylene oligomerization on Ni-Y and found a higher ethylene conversion and higher selectivity of diesel-range products (C6-C10+) with higher nickel content [23]. Hartmann et al.'s experiments showed the activity toward the formation of butenes increased with increasing nickel loading as acidity remained constant [91]. Martinez et al. increased nickel-exchange content in Ni-BEA from 1 to 2 wt.%, which also increased ethylene conversion [14]. The increased nickel content allowed the product C4 wt.% to remain high while feeding into acid chemistry and producing heavier products. The amount of dibranched product stayed at about 70 % of the total C8 distribution, suggesting the acid site is responsible for the dimerization of butenes to octenes. Recently in 2020, Chen et al. investigated Ni(II) ion-exchanged silica-alumina under various support treatments for ethylene oligomerization to produce C10+ for fuel production [81]. They concluded high Ni loading was more influential to produce C10+ oligomers than the support surface area and Brønsted acid amount. This suggests Ni-loading may be one of the most sensitive factors to consider in catalyst design.

Experimentally, other studies have shown that ethylene conversion and nickel activity increase sharply with increasing nickel content from about 2 wt.% before plateauing at about 5 wt.% (Fig. 11) [1,14,52,89].

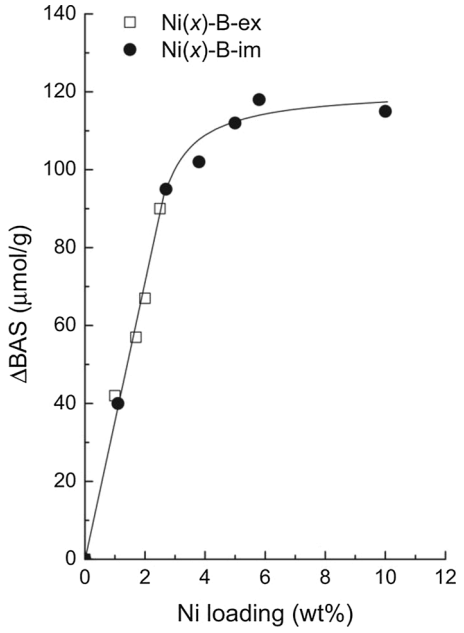

Fig. 11. Influence of Ni loading on ethylene conversion over Ni-BEA catalysts at: 393 K, 3.5 MPa total pressure, 2.6 MPa C_2H_4 pressure, 2.1 h^{-1} WHSV. Ion exchanged and impregnated samples were denoted as Ni(x)-B-ex and Ni(x)-B-im, respectively [14].

Likewise, on a Ni-silica-alumina catalyst, the dimer/trimer ratio decreased linearly with nickel content [17]. The ethylene conversion plateau may be due to highly loaded Ni catalysts containing blocked pores by bulk NiO particles, by being plugged by products, or due to high nickel coverage.

As the contribution of nickel sites increases, generally there is higher ethylene conversion and high selectivity towards linear alkenes, predominately butene, which can then undergo further acid-catalyzed chemistry. Altering the ratios between the two active sites could allow for fine-tuning of final products and remains an influential factor in coke prevention and catalyst stability [15,34,39].

4.3. Effect of metal-acid site distance

The position and dispersion of nickel and acid sites can lead to a "more efficient" bifunctional mechanism. Chen et al. tested catalysts with similar acid strength and Ni loading, but different aging temperature, which resulted in very different product fractions [81]. Chen et al. found the consecutive oligomerization of ethylene on Ni and acid sites was much more efficient in producing desirable C10+ products with increasing aging temperature. Using Ni-ion exchanged silica-alumina catalysts, by increasing the aging temperature, the dispersion and spatial ordering of the Ni was improved. A more uniform dispersion of Ni allows for a better match between Ni and acid active sites. This facilitates the transfer of one site's reaction intermediate to another. These closely matched Ni and acid active sites have been proposed to be a more efficient bifunctional mechanism (Fig. 12).

Forget et al. hypothesized that a nickel atom only requires a Brønsted acid site in close proximity to generate an active oligomerization site, and that there is no need to overwhelm nickel particles with the acidity often found in zeolites [33]. Using this logic, the group created a catalyst with nickel and silicon present on the aluminum-based support close to their stoichiometric loadings. The final catalysts were active, despite having low acidity and low metal loading, and at about 15 % butene conversion produced exclusively octenes.

While Chen et al. is one of the only studies currently published that benchmarked Ni-acid site distance, the dependence of metal-acid site distance on efficiency is a focus in the field of metal/acid hydrocracking. The efficiency of bifunctional metal-acid catalysts for hydrocracking has shown that mass transfer and site distance, which should be neither too close nor too far, can play an influential role [92–99]. Whether or not the significance of metal-acid distance also applies to nickel-acid oligomerization catalysts still remains to be addressed.

The nickel-acid distance may also be closely related to the support pore size. The effect of support pore size is discussed in the next section.

4.4. Effect of pore size

Porosity is another important factor that influences catalyst stability. Having wider pores allows for larger oligomers to move out of the support and reduces pore blocking. Smaller pores bring oligomers in close proximity with walls and active sites of the zeolite, leading to secondary reactions. In the same way, smaller pores allow for longer oligomers to be better stabilized than in larger pores. Thus, mesoporous catalysts are reported to have a longer lifetime and higher ethylene conversion than microporous catalysts [1,84]. However, it was found that catalytic activity is more closely related to acidity than pore structure at higher temperatures (> ~700 K) [63].

This effect can be better illustrated by comparing MCM studies. An approximate ranking of activity (from higher to lower activity) can be determined: Ni-MCM-48 > Ni-MCM-41 > Ni-Y > Ni-MCM-36 > Ni-MCM-22 [84,88,100]. Decreasing activity and selectivity for higher oligomer products align with decreasing accessibility of the structure and higher acidity (Table 3). MCM-48 has a three-dimensional, interconnected channel structure with larger pores, while MCM-41 has a one-dimensional channel system. MCM-36, on the other hand, has

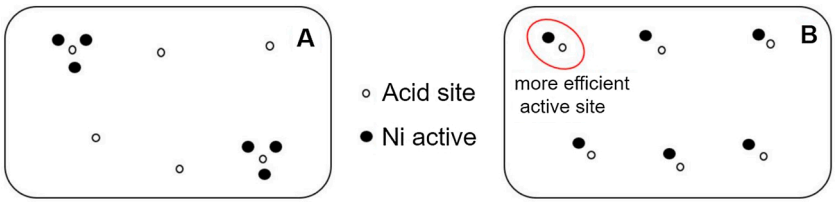

Fig. 12. Schematic of nickel and acid sites of (A) low degree of Ni dispersion and (B) high degree of Ni dispersion for formation of more efficient bifunctional active sites [81].

mesoporous and microporous properties, whereas, finally, MCM-22 has the most microporous structure (e.g. microporous surface area, pore diameter) out of those listed (Fig. 13). More mesoporous structures with moderate acidity, such as MCM-36, exhibit better catalytic activity and selectivity for even number oligomers than catalysts with more microporous structure and high acid site concentration, as in Ni-MCM-22 [5]. Alternatively, if high selectivity of a certain geometry, such as linear oligomers, is the main objective over activity, then a more microporous and shape selective support, such as Ni-MCM-22, yields almost exclusively dimerization and linear products. Outside of MCM studies done, similar pore size and deactivation trends have been found in comparisons of Ni-AlSBA-15 against Ni-Y and Ni-$AlSiO_2$ [56,85] as well as micro- and nano-crystalline Ni-BEA [34]. Tanaka et al. and Lallemand et al. also discuss pore size, in Ni-MCM-41 and Ni-Y, respectively [26,50]; but, both studies suggest that the Si/Ni ratio had greater effect on activity, where higher Si/Ni ratios exhibited greater reaction rate constants even accompanied with smaller pore size.

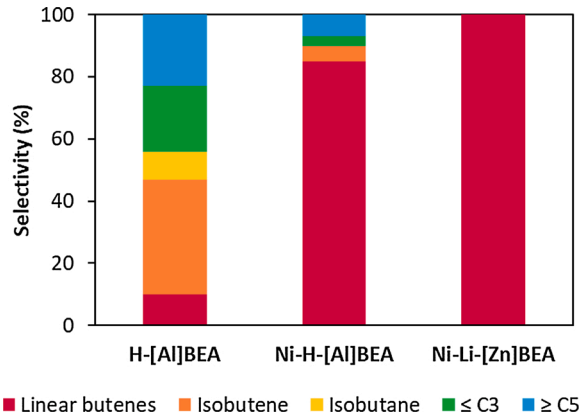

Fig. 14. Product molar selectivity from Joshi et al. 453 K, 0.4 kPa, ~1.4 % conversion [15]. H-[Al]BEA represents a catalyst with only active acid sites; Ni-H[Al]BEA a bifunctional Ni/acid zeolite with active nickel and acid sites; and Ni-Li-[Zn]BEA represents a nickel catalyst with only active nickel sites.

5. Tuning bifunctionality: a unified view on optimizing catalyst properties and reaction conditions

One of the most promising and intriguing properties of bifunctional Ni-acid catalysts is the ability to balance these two types of active sites to uniquely handle variable inputs or to shift product distributions. The balance between the nickel and acid site densities and reaction conditions are the key factors in manipulating the selectivity, activity, and stability of the catalyst.

Considering the Ni - acid together, the selectivity of bifunctional Ni - acid catalysts are towards more linear and more even carbon-numbered compounds than a purely acidic catalyst due to the nickel site's contribution (Fig. 14). On the other hand, the presence of Ni and acid sites allows the product distribution to break past the limiting Schulz-Flory distribution of a Ni-only catalyst. The relative nickel-to-acid contributions have a significant impact on catalyst performance and product distribution. This balance between Ni and acid site activity can be used to predict product distributions, as summarized in Fig. 15.

Typically, nickel site contributions are more pronounced at lower conversion (Section 3.1 [24,56,82,83]), lower temperature (Section 3.3 [14,56,63,79,84,87]), and higher nickel content (Section 4.2 [14,17,23,81,91]). A higher nickel site contribution generally means increased activity and lighter, even-numbered alkenes that will follow a Schulz-Flory-like distribution (Section 2.1). Also, at lower temperatures and higher pressures, bimolecular reactions, or in this case, oligomerization reactions, are favored [28].

Conversely, acid site contributions can be enhanced with higher conversion (Section 3.1 [24,56,82,83],), higher temperature (Section 3.3 [14,56,63,79,84,87],), and higher acid content or strength (Section 2.2 [17,64,83,84],). A higher acid site contribution will produce a broad distribution of branched alkenes, from C3 to C10+, and, in case of a sufficiently high temperature, alkanes, cyclic hydrocarbons, and aromatics (Section 2.2). Also, at higher temperatures and lower partial pressures, β-scission reactions are favored [28], potentially producing higher propene yields.

Well-dispersed nickel throughout the support can increase the number of active nickel sites and improve activity (Section 4.3 [33,81],). Porous supports that are more open and mesoporous are associated with more mild acidity and higher selectivity to even numbered oligomers (Section 4.4 [50,56,84,85,100],). Larger pores may also allow growth of molecules to larger sizes before blocking pores. Contrarily, more microporous and more acidic supports are associated with heavy, branched oligomers, and often coke, which are associated with blocked pores and deactivation.

Thus, heterogenous nickel-catalyzed olefin oligomerization can be

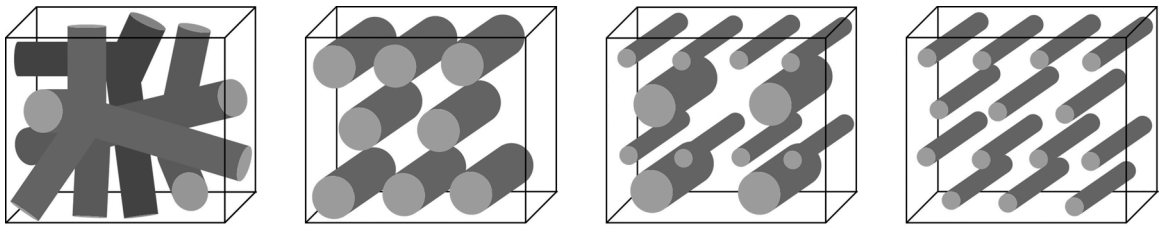

Fig. 13. Simplified and approximate porous structure highlighting the channels of (from left to right) MCM-48, MCM-41, MCM-36, MCM-22.

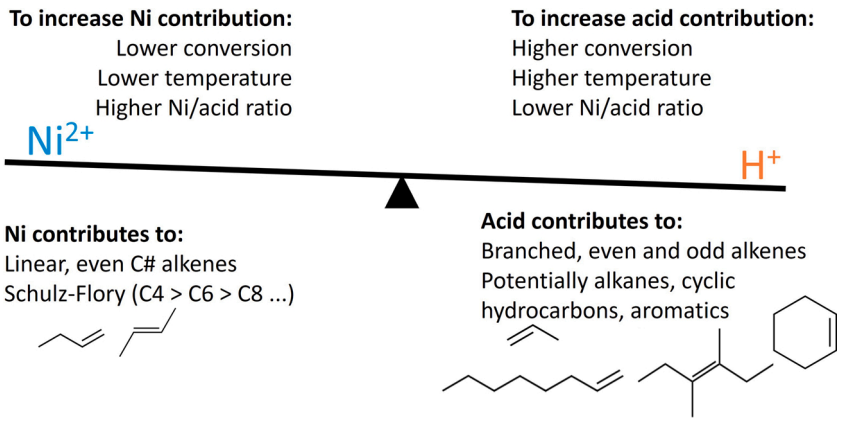

Fig. 15. Summary of effects and results of varying Ni/acid contributions for bifunctional optimization.

used similarly to how homogeneous nickel catalysts are used by utilizing minimal acid sites, just enough to create active oligomerization sites, and selectively produce linear dimerization products. On the other hand, heterogenous nickel-catalyzed olefin oligomerization can be used to create liquid range products by allowing acid chemistry to further oligomerize, the extent to which is then up to the user by balancing remaining reaction conditions or catalyst properties. Post-treatments to decrease surface acidity and open up porous structure, such as treatments with alkali ions, could give better stabilities while not affecting the activity or ethylene conversion too dramatically [7].

6. Concluding remarks

6.1. Conclusion

Due to recent research in the last five years, there have been significant insights into how nickel and acid sites work as a tandem for ethylene oligomerization. Across various experiments, models, and first-principles calculations, there has been considerable evidence supporting a Ni^{2+} site that can mobilize into a complex and oligomerize olefins via a Cossee-Arlman mechanism. The details of the Ni activation and deactivation remain uncertain, but it is likely that the active state is an anchored [alkene-Ni(II)-alkene]$^+$ complex affixed by two Ni-O bonds to the framework. The Ni complex can exchange framework ligand bonds with ethylene bonds to further grow an oligomer chain. The nickel site's insertion-termination mechanism produces a Schulz-Flory product distribution of predominantly butene and hexene. The dimerized or trimerized products from the nickel can be quickly catalyzed by Brønsted H^+ sites for further alkylation, isomerization, and cracking reactions.

Further investigations have led to a better understanding of how reaction conditions, including time-on-stream and temperature, as well as catalyst properties, including site concentrations and framework pore size, can impact the final product distributions. By adjusting contributions of these two types of sites, this catalyst can be uniquely adapted and tuned towards desirable product distributions. Generally, nickel site contributions are more pronounced at lower conversions, temperature, and pressure as well as higher nickel loading. Higher nickel site contributions often accompany increased activity and lighter, even carbon-number alkene products. Contrarily, acid site contributions dominate at higher conversion, temperature, pressure, acid concentration, and acid strength. Higher acid site contributions direct products towards classical acid oligomerization fractions, which include a broad distribution of even and odd alkenes and potentially alkanes, cyclic hydrocarbons, and aromatics, as well as potentially lower activity. The heterogenous support also impacts the catalytic behavior. More open, mesoporous structures with mild acidity align with higher activity and selectivity to even-numbered oligomers, whereas microporous and highly acidic supports tend to exhibit lower activity with heavy and branched oligomer products that can block pores.

6.2. Remaining uncertainties and future investigations

Even considering all the recent advances in understanding the Ni-acid mechanism discussed above (and in more detail in Section 2), there are still aspects that we are yet to fully grasp. For instance, activation of the Ni^{2+} Cossee-Arlman site remains ambiguous, difficult to observe, and possibly nuanced for different geometries of the support. First-principles studies to investigate and confirm the proposed Ni-activation and deactivation mechanisms are necessary. In combination with DFT studies, advanced characterizations under real reaction conditions (e.g., operando spectroscopies) can help understand the true nature of the active nickel sites as well as the activation and deactivation mechanisms.

Various reaction orders in alkene pressure have been experimentally observed depending on the support (see Section 2), suggesting that the surrounding framework and pore size hold influence over mechanistic details. These differences in reaction order could be due to the convolution of both the Ni and acid site consuming ethylene and producing butene. Likewise, it is possible this is the result of a simple coverage effect where the reaction is second order at low pressure and first order at sufficiently high pressure, often observed for Langmuir-Hinshelwood-Hougen-Watson type of mechanisms. Alternatively, this can be the complication of nickel co-dimerizing with species larger than ethylene. In kinetic modeling, the predicted coverages of species, including [ethyl-Ni-alkene]$^+$, is highly sensitive to the free energy of the species. This suggests that more detailed DFT calculations and kinetic models are required to fully understand the reaction orders.

Similarly, first-principles calculations can help answer remaining mechanistic questions, but no studies looking into the Ni-isomerization pathway to produce 2-butene nor of heterogenous nickel co-dimerization has been carried out. So, energy barriers that can quantify the likelihood of these pathways are still uncalculated. Additionally, systematically reporting the branching distribution of large alkene products obtained at high conversion could shed light into whether the nickel or acid site is responsible for further oligomerization events.

While experimental investigations into activation and reaction mechanisms have been made in the literature, generally there has not been the same pursuit into deactivation mechanisms. Experimental studies report deactivation but lack a molecular explanation apart from large oligomer products and coke blocking pores. For high nickel-loading, deactivation is likely caused predominantly by oligomer blockage (exponential deactivation) in mesoporous catalysts like Ni-MCM-41, but by neighboring nickel interactions (hyperbolic deactivation) in microporous catalysts like Ni-X (Section 3.2). Even in homogeneous nickel oligomerization, there are many different deactivation pathways depending on the system [7]. Thus, there could be potentially

different activation as well as deactivation mechanisms depending on active site distances or support porous system.

At the catalyst level, metal-acid optimal distance (discussed in Section 4.4) between the Ni and acid site for oligomerization catalysts remain largely unaddressed, although it is a potentially powerful tool to further tune the product distribution. There have been many studies on Ni-acid catalysts that vary nickel loading and acid concentration, yet there is no comprehensive study of how the distance between each type of active site or number of nickel/acid steps undergone by intermediates influences product distributions.

Overall, there is great flexibility of a Ni/acid bifunctional catalyst due to the many adjustable factors discussed, which gives this catalyst potential to be tuned to an "ideal" catalyst for a large range of applications. Despite lingering questions regarding active sites, mechanism, and deactivation, our understanding of not only how the product distributions of a Ni/acid catalyst change with changing conditions, but also why they change the way they do, has grown considerably within the last five years. Perhaps in the next five years these remaining uncertainties will be put to rest, and Ni/acid bifunctional heterogenous catalysts will have progressed from the lab bench and begun use for industrial ethylene oligomerization.

Funding sources

The National Science Foundation (NSF)Graduate Research Fellowship Program (GRFP) grant number DGE-1842165. Support from the NSF under Cooperative Agreement No. EEC-1647722. Support from the Belgium American Education Fellowship (BAEF). Support from Special Research Fund of Ghent University (grant number BOF/PDO/2018/001901).

Declaration of Competing Interest

The authors declare that they have no known competing financial interests or personal relationships that could have appeared to influence the work reported in this paper.

Acknowledgments

P.S.F. Mendes would like to thank M. Fernanda N.N. Carvalho for having introduced him to the amazing world of nickel catalysis.

References

[1] A. Finiels, F. Fajula, V. Hulea, Catal. Sci. Technol. 4 (2014) 2412–2426.
[2] N.M. Eagan, M.D. Kumbhalkar, J.S. Buchanan, J.A. Dumesic, G.W. Huber, Nat. Rev. Chem. 3 (2019) 223–249.
[3] O. Muraza, Ind. Eng. Chem. Res. 54 (2015) 781–789.
[4] O. Jan, F.L.P. Resende, Fuel Process. Technol. 179 (2018) 269–276.
[5] H. Zhang, X. Li, Y. Zhang, S. Lin, G. Li, L. Chen, Y. Fang, H. Xin, X. Li, Energy Environ. Focus 3 (2014) 246–256.
[6] V. Hulea, ACS Catal. 8 (2018) 3263–3279.
[7] H. Olivier-Bourbigou, P.A.R. Breuil, L. Magna, T. Michel, M.F. Espada Pastor, D. Delcroix, Chem. Rev. 120 (2020) 7919–7983.
[8] W. Keim, Angew. Chem. Int. Ed. 52 (2013) 12492–12496.
[9] B. Reuben, H. Wittcoff, J. Chem. Educ. 65 (1988) 605–607.
[10] G.P. Belov, P.E. Matkovsky, Pet. Chem. U S S R 50 (2010) 283–289.
[11] R.J. Quann, L.A. Green, S.A. Tabak, F.J. Krambeck, Ind. Eng. Chem. Res. 27 (1988) 565–570.
[12] K.G. Wilshier, Stud. Surf. Sci. Catal. 36 (1988) 621–625.
[13] W. Monama, E. Mohiuddin, B. Thangaraj, M.M. Mdleleni, D. Key, Catal. Today 342 (2020) 167–177.
[14] A. Martínez, M.A. Arribas, P. Concepción, S. Moussa, Appl. Catal. A Gen. 467 (2013) 509–518.
[15] R. Joshi, G. Zhang, J.T. Miller, R. Gounder, ACS Catal. 8 (2018) 11407–11422.
[16] I.E. Maxwell, Adv. Catal. 31 (1982) 1–76.
[17] R.L. Espinoza, R. Snel, C.J. Korf, C.P. Nicolaides, Appl. Catal. 29 (1987) 295–303.
[18] P.S.F. Mendes, J.M. Silva, M.F. Ribeiro, A. Daudin, C. Bouchy, Catal. Today 356 (2020) 260–270.
[19] A. John Kolombos, United States Patent (US-4112011-A), British Petroleum Co., OLIGOMERIZATION PROCESS, 1977.
[20] C. Shao, W.H. Sun, Z. Li, Y. Hu, L. Han, Catal. Commun. 3 (2002) 405–410.
[21] Y. Chauvin, D. Commereuc, F. Hugues, J. Thivolle-cazat, Appl. Catal. 42 (1988) 205–216.
[22] J. Heveling, C.P. Nicolaides, M.S. Scurrell, Appl. Catal. A Gen. 173 (1998) 1–9.
[23] J. Heveling, A. van der Beek, M. de Pender, Appl. Catal. 42 (1988) 325–336.
[24] F.T.T. Ng, D.C. Creaser, Appl. Catal. A Gen. 119 (1994) 327–339.
[25] F.T.T. Ng, D.C. Creaser, Stud. Surf. Sci. Catal. 73 (1992) 123–131.
[26] M. Lallemand, A. Finiels, F. Fajula, V. Hulea, Appl. Catal. A Gen. 301 (2006) 196–201.
[27] M. O'Connor, C.T. Kojima, Catal. Today 6 (1990) 329–349.
[28] M. Ghashghaee, Int. Rev. Chem. Eng. 34 (2018) 595–655.
[29] CISTAR, CISTAR, Center for Innovative and Strategic Transformation of Alkane Resources, 2018. Available at: https://citstar.us/ (Access: 1st Jan 2018).
[30] RAPID Funded Projects RAPID Manufacturing Institute for Process Intensification. Available at: https://www.aiche.org/rapid/projects/list?field_focus_area_tid%5B%5D=l18146&title=#views-exposed-form-rapid-projects-page. (Accessed: 28th August 2019).
[31] University of Ghent. Ocmol., 2014. Available at: http://www.ocmol.eu/index.php. (Accessed: 28th August 2019).
[32] J. Heveling, C.P. Nicolaides, M.S. Scurrell, Catal. Letters 95 (2004) 87–91.
[33] S. Forget, H. Olivier-Bourbigou, D. Delcroix, Chem. Cat. Chem. 9 (2017) 2408–2417.
[34] R. Henry, M. Komurcu, Y. Ganjkhanlou, R.Y. Brogaard, L. Lu, K.J. Jens, G. Berlier, U. Olsbye, Catal. Today 299 (2018) 154–163.
[35] S. Moussa, P. Concepción, M.A. Arribas, A. Martínez, ACS Catal. 8 (2018) 3903–3912.
[36] R.Y. Brogaard, U. Olsbye, ACS Catal. 6 (2016) 1205–1214.
[37] R.Y. Brogaard, M. Kømurcu, M.M. Dyballa, A. Botan, V. Van Speybroeck, U. Olsbye, K. De Wispelaere, ACS Catal. 9 (2019) 5645–5650.
[38] K. Toch, J.W. Thybaut, G.B. Marin, Appl. Catal. A Gen. 489 (2015) 292–304.
[39] K. Toch, J.W. Thybaut, M.A. Arribas, A. Martínez, G.B. Marin, Chem. Eng. Sci. 173 (2017) 49–59.
[40] E.D. Metzger, R.J. Comito, C.H. Hendon, M. Dincă, J. Am. Chem. Soc. 139 (2017) 757–762.
[41] V. Bernales, A.B. League, Z. Li, N.M. Schweitzer, A.W. Peters, R.K. Carlson, J. T. Hupp, C.J. Cramer, O.K. Farha, L. Gagliardi, J. Phys. Chem. C 120 (2016) 23576–23583.
[42] C. Bianchini, G. Giambastiani, I.G. Rios, G. Mantovani, A. Meli, A.M. Segarra, Coord. Chem. Rev. 250 (2006) 1391–1418.
[43] P.-A.R. Breuil, L. Magna, H. Olivier-Bourbigou, Catal. Letters 145 (2015) 173–192.
[44] A. Forestière, H. Olivier-Bourbigou, L. Saussine, Oil Gas Sci. Technol. IFP 64 (2009) 649–667.
[45] Y. Ganjkhanlou, E. Groppo, S. Bordiga, M.A. Volkova, G. Berlier, V. Hulea, F. Fajula, F.T.T. Ng, D.C. Creaser, Appl. Catal. A Gen. 225 (2016) 213–222.
[46] M. Lallemand, A. Finiels, F. Fajula, V. Hulea, J. Phys. Chem. C 113 (2009) 20360–20364.
[47] J. Xu, R. Wang, L. Zheng, J. Ma, W. Yan, X. Yang, J. Wang, X. Su, Y. Huang, Catal. Sci. Technol. 11 (2021) 1510–1518.
[48] I. Agirrezabal-Telleria, E. Iglesia, J. Catal. 389 (2020) 690–705.
[49] A.N. Mlinar, G.B. Baur, G.G. Bong, A. Getsoian, A.T. Bell, J. Catal. 296 (2012) 156–164.
[50] M. Tanaka, A. Itadani, Y. Kuroda, M. Iwamoto, J. Phys. Chem. C 116 (2012) 5664–5672.
[51] A. Lacarriere, J. Robin, D. Świerczyński, A. Finiels, F. Fajula, F. Luck, V. Hulea, Chem. Sus. Chem. 5 (2012) 1787–1792.
[52] I. Agirrezabal-Telleria, E. Iglesia, J. Catal. 352 (2017) 505–514.
[53] S.L.C. Moors, K. De Wispelaere, J. Van Der Mynsbrugge, M. Waroquier, V. Van Speybroeck, ACS Catal. 3 (2013) 2556–2567.
[54] C. Paolucci, I. Khurana, A.A. Parekh, S. Li, A.J. Shih, H. Li, J.R. Di Iorio, J. D. Albarracin-Caballero, A. Yezerets, J.T. Miller, W.N. Delgass, F.H. Ribeiro, W. F. Schneider, R. Gounder, Science 357 (2017) 898–903.
[55] P. Serna, B.C. Gates, J. Am. Chem. Soc. 133 (2011) 4714–4717.
[56] R.D. Andrei, M.I. Popa, F. Fajula, V. Hulea, J. Catal. 323 (2015) 76–84.
[57] M. Ghambarian, M. Ghashghaee, Z. Azizi, M. Balar, Struct. Chem. 30 (2019) 137–150.
[58] R. Joshi, A. Saxena, R. Gounder, Catal. Sci. Technol. 10 (2020) 7101–7123.
[59] J. Liu, J. Ye, Z. Li, K.I. Otake, Y. Liao, A.W. Peters, H. Noh, D.G. Truhlar, L. Gagliardi, C.J. Cramer, O.K. Farha, J.T. Hupp, J. Am. Chem. Soc. 140 (2018) 11174–11178.
[60] V. Tognetti, A. Buchard, A. Auffrant, I. Ciofini, P. Le Floch, C. Adamo, J. Mol. Model. 19 (2013) 2107–2118.
[61] H.B. Gray, C.J. Ballhausen, J. Am. Chem. Soc. 85 (1963) 260–265.
[62] E.D. Metzger, R.J. Comito, Z. Wu, G. Zhang, R.C. Dubey, W. Xu, J.T. Miller, M. Dinca, ACS Sustain. Chem. Eng. 7 (2019) 6654–6661.
[63] F. Jin, Y. Yan, G. Wu, Catal. Today 355 (2020) 148–161.
[64] K. Lu, F. Jin, G. Wu, Y. Ding, Sustain. Energy Fuels 3 (2019) 3569–3581.
[65] M. Iwamoto, Molecules 16 (2011) 7844–7863.
[66] V. Hulea, Catal. Sci. Technol. 9 (2019) 4466–4477.
[67] A.S. Frey, O. Hinrichsen, Microporous Mesoporous Mater. 164 (2012) 164–171.
[68] T. Lehmann, T. Wolff, V.M. Zahn, P. Veit, C. Hamel, A. Seidel-Morgenstern, Catal. Commun. 12 (2011) 368–374.
[69] L.A. Perea, M. Felischak, T. Wolff, C. Hamel, A. Seidel-Morgenstern, Chem. IngenieurTechnik 89 (2017) 903–914.
[70] M. Stoyanova, M. Schneider, M.M. Pohl, U. Rodemerck, Catal. Commun. 92 (2017) 65–69.

[71] M. Felischak, T. Wolff, L. Alvarado Perea, A. Seidel-Morgenstern, C. Hamel, Chem. IngenieurTechnik 92 (2020) 564–574.
[72] C.P. Nicholas, Appl. Catal. A Gen. 543 (2017) 82–97.
[73] M.N. Mazar, S. Al-Hashimi, M. Cococcioni, A. Bhan, J. Phys. Chem. C 117 (2013) 23609–23620.
[74] J.S. Buchanan, J.G. Santiesteban, W.O. Haag, J. Catal. 158 (1996) 279–287.
[75] A. Ehrmaier, Y. Liu, S. Peitz, A. Jentys, Y.H.C. Chin, M. Sanchez-Sanchez, R. Bermejo-Deval, J. Lercher, ACS Catal. 9 (2019) 315–324.
[76] L. Bonneviot, D. Olivier, M. Che, J. Mol. Catal. 21 (1983) 415–430.
[77] D. Kiessling, G.F. Froment, Appl. Catal. 71 (1991) 123–138.
[78] M.D. Heydenrych, C.P. Nicolaides, M.S. Scurrell, J. Catal. 197 (2001) 49–57.
[79] Q. Zhang, I.G. Dalla Lana, Chem. Eng. Sci., Elsevier Science Ltd, 1997, pp. 4187–4195.
[80] L. Riekert, J. Catal. 19 (1970) 8–14.
[81] L. Chen, G. Li, Z. Wang, S. Li, M. Zhang, X. Li, Catalysts 10 (2020) 24–30.
[82] O. Jan, K. Song, A. Dichiara, F.L.P. Resende, Ind. Eng. Chem. Res. 57 (2018) 10241–10250.
[83] S. Moussa, M.A. Arribas, P. Concepción, A. Martínez, Catal. Today 277 (2016) 78–88.
[84] M. Lallemand, O.A. Rusu, E. Dumitriu, A. Finiels, F. Fajula, V. Hulea, Appl. Catal. A Gen. 338 (2008) 37–43.
[85] R.D. Andrei, E. Borodina, D. Minoux, N. Nesterenko, J.P. Dath, C. Cammarano, V. Hulea, Ind. Eng. Chem. Res. 59 (2020) 1746–1752.
[86] A.N. Mlinar, S. Shylesh, O.C. Ho, A.T. Bell, G.B. Baur, G.G. Bong, A. Getsoian, A. T. Bell, J. Catal. 4 (2014) 337–343.
[87] V. Hulea, F. Fajula, J. Catal. 225 (2004) 213–222.
[88] V. Hulea, M. Lallemand, A. Finiels, F. Fajula, Stud. Surf. Sci. Catal., Elsevier Inc., 2005, pp. 1621–1628.
[89] C.P. Nicolaides, M.S. Scurrell, P.M. Semano, Appl. Catal. A Gen. 245 (2003) 43–53.
[90] C. Wang, L. Wang, G. Wu, F. Jin, X. Zhan, Y. Ding, Catal. Letters 150 (2020) 429–437.
[91] M. Hartmann, A. Pöppl, L. Kevan, J. Phys. Chem. 100 (1996) 9906–9910.
[92] R. Brosius, J.C.Q. Fletcher, J. Catal. 317 (2014) 318–325.
[93] J. Francis, E. Guillon, N. Bats, C. Pichon, A. Corma, L.J. Simon, Appl. Catal. A Gen. 409–410 (2011) 140–147.
[94] J. Zecevic, G. Vanbutsele, K.P. De Jong, J.A. Martens, Nature 528 (2015) 245–254.
[95] Y. Zhang, D. Liu, Z. Men, K. Huang, Y. Lv, M. Li, B. Lou, Fuel 236 (2019) 428–436.
[96] K. Cheng, L.I. Wal, H. Yoshida, J. Oenema, J. Harmel, Z. Zhang, G. Sunley, J. Zečević, K.P. Jong, Angew. Chem. 132 (2020) 3620–3628.
[97] P.B. Weisz, Adv. Catal. 13 (1962) 137–190.
[98] N. Batalha, L. Pinard, C. Bouchy, E. Guillon, M. Guisnet, J. Catal. 307 (2013) 122–131.
[99] P.S.F. Mendes, J.M. Silva, M.F. Ribeiro, A. Daudin, C. Bouchy, Chem. Cat. Chem. 12 (2020) 4582–4592.
[100] M. Lallemand, A. Finiels, F. Fajula, V. Hulea, Stud. Surf. Sci. Catal. 170 (2007) 1863–1869.